Calcium Site Mutations in Cadherin: Impact on Adhesion and Evidence of Cooperativity†

A. Prakasam,‡ Y.-H. Chien,§ V. Maruthamuthu,‡ and D. E. Leckband*,‡,§,||,⊥

Department of Chemical and Biomolecular Engineering, Department of Biochemistry, Department of Chemistry, and Center for Biophysics and Computational Biology, University of Illinois at Urbana−Champaign, Urbana, Illinois 61801

Received February 1, 2006; Revised Manuscript Received April 10, 2006

ABSTRACT: This work describes quantitative force and bead aggregation measurements of the adhesion and binding mechanisms of canine E-cadherin mutants W2A, D134A, D103A, D216A, D325A, and D436A. The W2A mutation affects the formation of the N-terminal strand dimer, and the remaining mutations target calcium binding sites at the interdomain junctions. Surface force measurements show that the full ectodomain of canine E-cadherin forms two bound states that span two intermembrane gap distances. The outer bond coincides with adhesion between the N-terminal extracellular domains (EC1) and the inner bond corresponds to adhesion via extracellular domain 3 (EC3). The W2A, D103A, D134A, and D216A mutations all eliminated adhesion between the N-terminal domains, and they attenuated or nearly eliminated the inner bond. The W2A mutant, which does not destabilize the protein structure, attenuates binding via EC3, which is separated from the mutation by several hundred amino acids. This long-range effect suggests that the presence or absence of tryptophan-2 docking allosterically alters the adhesive function of distal sites on the protein. This finding appears to reconcile the multidomain binding mechanism with mutagenesis studies, which suggested that W2 is the sole binding interface. The effects of the calcium site mutations indicate that structural perturbations cooperatively impact large regions of the protein structure. However, the influence of the calcium sites on cadherin structure and function depends on their location in the protein.

Cadherins are calcium dependent cell adhesion glycoproteins. Different members of the cadherin superfamily are expressed in different tissues in a spatiotemporal fashion during development (*1*−*4*). They are essential for embryogenesis and tissue morphogenesis. Cadherins also maintain the structural integrity and regulate the reorganization of adult soft tissues. Abnormal cadherin function occurs in many types of cancers (*4*−*6*).

Epithelial cadherin (ECAD) promotes homophilic cell adhesion and inhibits motility in normal tissues, although its expression is not confined to the epithelium. Cadherin mutations and abnormal cadherin expression are associated with several malignant carcinomas (*6*). In some colon and esophageal cancers, E-cadherin is downregulated. Other diffuse-type gastric cancers are attributed to molecular level changes due to point mutations in the cadherin extracellular domains. In particular, the point mutant D216A occurs in some highly metastatic tumors (*5*, *6*).

Classical cadherins comprise an extracellular segment containing five, tandemly arranged extracellular (EC)[1] domains, a transmembrane domain, and a highly conserved cytoplasmic domain (*7*) (Figure 1a). The cadherin cytoplasmic domain binds catenins and may interact with the actin cytoskeleton. Calcium ions stiffen the cadherin ectodomain by complexing conserved binding motifs at the junctions between the EC domains (*8*−*11*).

The importance of the EC1 domain for cadherin adhesion is well established. Based on structural studies and site directed mutagenesis, the binding mechanism is postulated to involve either the reciprocal insertion of tryptophan-2 side chains (W2) into the hydrophobic pockets on opposed EC1 domains (*10*, *12*) or the exchange between adjacent proteins to form cis dimers followed by trans binding (*13*−*15*). Mutating the W2 residue or amino acids in the hydrophobic binding pocket eliminated cell aggregation in stirred (agitated) cell suspensions and cadherin-mediated bead adsorption in flow assays (*16*−*19*). The N-terminal domain also appears to determine the binding specificity since exchanging

† This work was supported by NIH Grant 5 RO1 GM51338.

* Address correspondence to this author. Mailing address: Department of Chemical and Biomolecular Engineering and Department of Chemistry, 600 South Mathews Avenue, Urbana, IL 61801. Phone: 217-244-0793. Fax: 217-333-5052. E-mail: Leckband@uiuc.edu.

‡ Department of Chemical and Biomolecular Engineering.

§ Department of Biochemistry.

|| Department of Chemistry.

⊥ Center for Biophysics and Computational Biology.

[1] Abbreviations: ECAD, epithelial cadherin; CCAD, *Xenopus* cleavage stage cadherin; EEC1−5, extracellular domains one through five of epithelial cadherin; EEC1−5Fc, extracellular domains one through five with a C-terminal Fc tag; EC12 extracellular domains one and two; DPPE, 1,2-dipalmitoyl-*sn*-glycero-3-phosphoethanolamine; DLPE, 1,2-dilauryl-*sn*-glycero-3-phosphoethanolamine; DTPC, 1,2-ditridecanoyl-*sn*-glycero-3-phosphocholine; NTA-DLGE, 6-[9-[2,3-bis(dodecyloxy)propyl]-3,6,9-trioxanonyl-1-oxycarboxylamino]-2-[di(carboxymethyl)amino]hexanoic acid; PCR, polymerase chain reaction; BSA, bovine serum albumin; SFA, surface force apparatus; SPR, surface plasmon resonance; CD, circular dichroism.

10.1021/bi060213m CCC: $33.50
Published on Web 05/16/2006

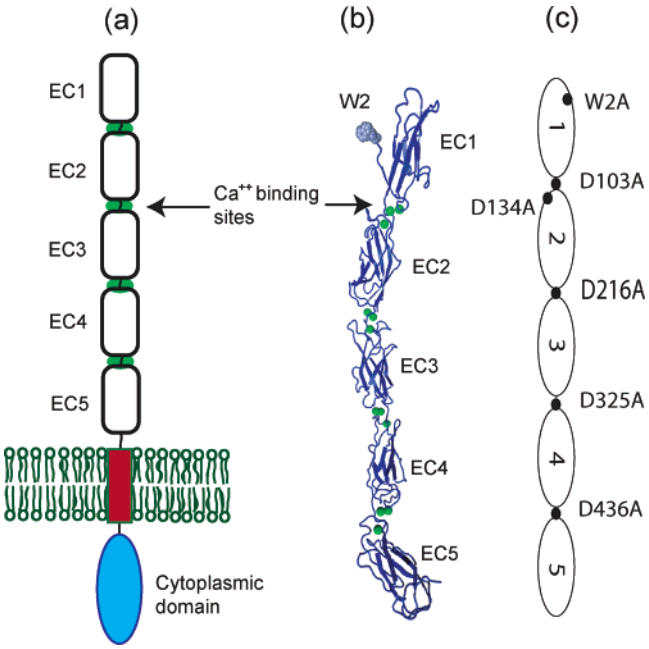

FIGURE 1: (a) Architecture of classical cadherins showing the five extracellular domains EC1−5, the transmembrane domain, and the cytoplasmic domain. (b) Crystal structure of the extracellular region showing the W2 residue (blue van der Waals structure) and 12 calciums (green balls). (c) Identities and locations of the E-cadherin point mutations at W2, D134, D103, D216, D325, and D436 studied in this work.

the N-terminal domain of E-cadherin with the EC1 domain of N-cadherin switched the binding specificity (*20, 21*).

Several studies implicate other EC domains in cadherin adhesion. Direct molecular force measurements showed that *Xenopus* cleavage stage C-cadherin forms three adhesive bonds, and at least one of these involves EC3 (*22*−*24*). These results are supported by single bond rupture measurements of both human E-cadherin and *Xenopus* C-cadherin (*25, 26*). The latter results show that strong adhesion requires more than the EC12 domains. Cell adhesion studies with C-cadherin deletion mutants showed that strong adhesion requires more than the outer EC12 segment (*27*). Conversely, cells that express cadherin lacking EC1 weakly coaggregated cells that express the wild-type protein (*28*). Finally, cancer-associated mutations are found throughout the extracellular domain, but there is a mutation hot spot in E-cadherin between EC2 and EC3 associated with gastric cancer (*29*). One point mutant, D216A, affects the calcium-binding site at this junction.

Cadherin extracellular domains bind three calcium ions at each of four EC domain junctions (*8, 10, 15*) (Figure 1b). Calcium binding maintains the structural rigidity, adhesive activity, and protease resistance of cadherin ectodomains. At $[Ca^{2+}] > 50\ \mu M$, cadherin becomes an elongated semiflexible rod, but only $[Ca^{2+}] > 0.5$ mM activates the adhesive function (*15, 30*). However, one Ca^{2+} site at the EC1/EC2 junction has a lower affinity than the other sites, and this low affinity site appears to regulate the adhesive activity (*11, 15, 30*).

Recent studies suggest structural cooperativity between the W2 binding pocket and the D134 calcium-binding site (*12*). That is, structural changes due to ligand binding or mutations induce nonlocal perturbations in the structure. Either low calcium or the D134A mutation causes the W2 side chain to bind preferentially to the hydrophobic pocket of its own molecule rather than an adjacent protein (*11, 12, 15*). In addition, there is cooperativity between the three calcium sites at the EC1/EC2 junction (*31*).

In cell adhesion and motility studies (*32*), point mutations at the DXXD → Ca^{2+} binding motifs at the EC12 and EC23 junctions caused improper cadherin localization and diminished cell adhesion. Mutations at the EC34 and EC45 junctions did not significantly affect either cell aggregation or protein localization. The tumor associated DXXD → DXXA mutation D216A at the EC23 junction increased cell motility. Another mutation, D134A, at the DAD motif (DAD → AAD) in the EC12 junction abolished adhesion.

In this investigation, we used direct force measurements and bead aggregation assays to assess the impact of the W2A and calcium binding site mutations on the molecular mechanism of cadherin adhesion. This study focuses on the E-cadherin ectodomain mutants W2A, D103A, D134A, D216A, D325A, and D436A. Canine E-cadherin ectodomains form two adhesive complexes that span two membrane gap distances. Several mutations affect both bonds, and this suggests that the effects of structural perturbations propagate over large distances in the protein. The effect of the W2A mutant suggests that the Trp2 side chain docking allosterically modulates the adhesive activity of the EC3 domain. The structural cooperativity exhibited by these mutants is a logical property of large cell adhesion molecules, which transmit mechanical signals over large distances to the cytoplasmic domains. The force measurements also reveal molecular level changes associated with altered cell adhesion and motility in gastric cancers caused by these mutations.

MATERIALS AND METHODS

Chemicals. 1,2-Dipalmitoyl-*sn*-glycero-3-phosphoethanolamine (DPPE) and 1,2-ditridecanoyl-*sn*-glycero-3-phosphocholine (DTPC) were obtained from Avanti Polar Lipids (Alabaster, AL). 6-[9-[2,3-Bis(dodecyloxy)propyl]-3,6,9-trioxanonyl-1-oxycarboxylamino]-2-[di(carboxymethyl)amino]hexanoic acid (NTA-TRIG-DLGE) was custom synthesized by Northern Lipids (Vancouver, BC). Tris buffer was purchased from Sigma (St. Louis, MO), and all high purity salts were from Aldrich (St. Louis, MO).

E-Cadherin Constructs. The plasmid pcDNA3.1 encoding full length ectodomains of canine E-cadherin fused to the Fc domain of human IgG (a gift from Prof. James Nelson, Stanford University) has been described (*33*). The point mutants were created using the QuikChange site-directed mutagenesis kit (Stratagene, La Jolla, CA) according to the manufacturer's protocol. We thus generated the N-terminal W2A mutation and mutations at the calcium binding motifs at the EC12 (D103A and D134A), EC23 (D216A), EC34 (D325A), and EC45 (D436A) junctions (Figure 1c). Forward primers for the mutants were designed using the Stratagene labtools software and were used in conjunction with their reverse compliments. The forward primers used were as follows:

W2A: 5′-AGAAGACAGAAGAGAGACGCGGTT ATCCCTCCTATCAG-3′

D103A: 5′-CGGTGACAGATCAGAATGCAAA CAAGCCCGAGTTCACC-3′

D134A: 5′-CAGGTGACAGCCACAGCAGCGGA TGATGATGTGA-3′

D216A: 5′-AGTCACTGACATCAATGCAAA CCCCCCCATCTTCAACC-3′

D325A: 5′-CACTGTGGACGTGGAAG(C)TGTG AATGAAGCC″-3′

D436A: 5′-CTCTCTGATGTGAATG(C)CAATG GCCCCATTCC-3′

The plasmid encoding each point mutant was prepared by polymerase chain reaction (PCR) using *Pfu* Turbo DNA polymerase supplied with the QuikChange site-directed mutagenesis kit (Stratagene, La Jolla, CA). *Pfu Turbo* DNA polymerase extends and incorporates the mutagenic primers, resulting in nicked circular strands. At the end of the temperature cycle, the nonmutated parental DNA template was digested with *Dpn*I. Supercompetent XL1-Blue E-coli (Stratagene) was then transformed with the thus generated mutated, circular, nicked dsDNA, and plated overnight on LB-ampicillin agar plates. The XL1-Blue cells repair the nicks in the mutated plasmid after the transformation (Stratagene instruction manual). Several colonies were isolated and expanded by culturing in LB-ampicillin medium for ~4 h at 37 °C. The plasmid DNA from each colony was isolated and purified using the Qiagen miniprep kit (Qiagen Inc., Valencia, CA). To confirm that the point mutations were properly generated at the correct location and that the insert was of the correct orientation and size, the plasmids were restricted using *Eco*RV/*Xba*I endonucleases and analyzed by 0.6% agarose gel electrophoresis. Two fragments of ~5.4 kb and ~2.8 kb, corresponding to the plasmid and insert, respectively, were generated, with plasmids from colonies having the correct insert. In addition to the mutation sites, we sequenced the first 1600 bases of the DNA, that is, the first three domains plus the prosequence (W. M. Keck Center for Comparative and Functional Genomics, University of Illinois at Urbana−Champaign). This verified the fidelity of the selected clone and the introduced mutation.

Expression and Purification of E-Cadherin Mutants. For each mutant, HEK293 cells (CRL1573, ATCC) were stably transfected with the corresponding plasmid DNA, using Lipofectamine 2000 (Invitrogen Inc., Carlsbad, CA) according to the manufacturer's protocol. The transfections were performed in a six-well plate with 293 cells which were >90% confluent. The DNA (μg):lipofectamine (μL) ratio used was between 1:1 and 1:5. Individual colonies were isolated after 10−14 days under selection with 0.4 mg/mL Geneticin (Invitrogen, Carlsbad, CA). The clones with the highest protein expression levels were detected by Western blot (ECL Western Blot Analysis System, Amersham Biosciences, Uppsala, Sweden) using an anti-human IgG HRP conjugate (Promega, Madison, WI). The selected clones were cultured in DMEM containing 10% FBS and 0.4 mg/mL Geneticin. During the protein collection phase, the cultures were switched to serum free DMEM, in order to simplify the subsequent protein purification and to increase protein yields. The mutants were purified from the filtered serum-free conditioned medium by affinity chromatography using Protein-A Affigel (BioRad, Hercules, CA) (*33*). The protein purity was assessed by SDS−PAGE on a 7.5% gel and staining with Coomassie Blue dye (Figure 2). In some cases, in addition to the mature form of the cadherin, an additional band of slightly higher molecular weight eluted in the ECAD fraction. However, passing the concentrated ECAD fraction over the affinity column a second time produced pure ECAD. Although the additional, higher molecular weight band could be a fraction of the expressed cadherin retaining the N-terminal pro-domain (*33*), this is unlikely given its removal by the second affinity column.

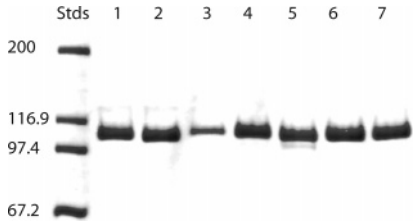

FIGURE 2: 7% SDS−PAGE of E-cadherin variants. Lane 1 shows broad range molecular weight standards and corresponding molecular weights in kilodaltons. Lanes 1−7 contain, in order, D436A, D325A, D216A, D134A, D103A, W2A, and wild-type Fc-tagged ectodomains.

Circular Dichroism Measurements. The protein fragments were characterized by circular dichroism with a Jasco 720 spectrometer in the Laboratory for Fluorescence Dynamics at the University of Illinois. Solutions of 0.2 mg/mL protein were scanned three times from 200 to 350 nm at a rate of 50 nm/min. The spectra were normalized by the protein concentrations for comparison. Spectra were analyzed according to published protocols (*34*) by using CONTIN software (*35*).

Bead Aggregation Assays. The functional activity of the cadherin point mutants was tested by their ability to aggregate 1 μm diameter fluorescent microspheres (Bangs Laboratories Inc., Fishers, IN). In these assays, protein binding induces particle aggregation, and collisions result from Brownian motion. The latex microsphere surface was chemically modified with NTA (nitrilo triacetic acid) groups as described previously (*23*). A 2 μg aliquot of activated beads was incubated with 5 μM protein A in 50 mM Tris, 100 mM $NaNO_3$, 50 μM $NiSO_4$, and 2 mM $Ca(NO_3)_2$ at pH 7.6 for 1 h at room temperature. The unreacted protein A was removed by centrifuging and washing the beads. The protein A conjugated beads were then resuspended in buffer, and 0.4 μg of Fc-tagged cadherin in 50 mM Tris, 100 mM $NaNO_3$, 50 μM $NiSO_4$, and 2 mM $Ca(NO_3)_2$ was added. Identical conditions were used for all cadherin mutants, and the measurements were carried out on the same day with the same batch of protein A modified beads. Thus, variations in aggregation are attributed to differences between the proteins and not to variations in conditions such as protein density or bead preparations. The cadherin was incubated with the beads at room temp for 30 min, and the aggregate sizes were then imaged with a Zeiss Axiovert 100 research grade inverted fluorescence microscope, using the 40× objective. Two independent experiments were conducted with all variants, and triplicate samples were prepared in a given experiment. Several images of the bead preparation were

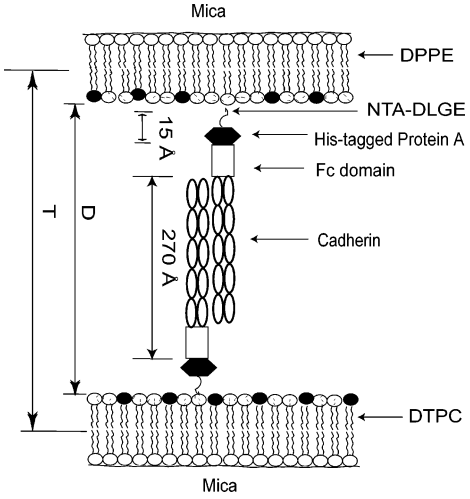

FIGURE 3: Sample configuration used SFA measurements. Recombinant canine E-cadherin ectodomains are immobilized on opposed supported lipid bilayers by an engineered C-terminal Fc domain. The lipid bilayer consiststs of a gel phase DPPE layer and an outer fluid phase DLGE-NTA monolayer. The Fc-cadherin ectodomains are anchored to the membrane by an immobilized histidine tagged protein A fragment. *T* is the absolute distance between the outer surfaces of the DPPE monolayers. *D* is the absolute separation between the surfaces of the two lipid bilayers.

taken to ensure that the images were representative of the sample. Wild-type E-cadherin was used as a positive control, while bovine serum albumin (BSA) and calcium-free buffer were negative controls.

Surface Force Measurements. The hallmark of the surface force apparatus (SFA) technique is its ability to measure integrated force between two opposed surfaces as a function of the absolute distance between them (*36*). In these measurements, $D = 0$ corresponds to contact between two opposed bilayer membranes on which the cadherins are bound (Figure 3). In order to calibrate $D = 0$, two DPPE monolayers supported on mica sheets are brought into contact in air. The wavelengths of the interference fringes at DPPE contact give the absolute thicknesses of the mica sheets and DPPE monolayers (*37*). The outer NTA-DLGE lipid layer and cadherin monolayers are then deposited onto the DPPE. The resulting change in the wavelengths of the interference fringes at the distance of closest approach gives the thickness *T* of the deposited lipid and cadherin monolayers (Figure 3). The absolute separation *D* between the bilayers is then $D = T - T_{NTA-DLGE}$, where $T_{NTA-DLGE}$ is the measured thickness of the NTA-DLGE monolayer (*23*, *24*, 38).

We used the Mark II surface force apparatus (SFA) to measure the normalized force between oriented Fc-tagged cadherin molecules coated on the two macroscopic surfaces as a function of the absolute separation *D* between the supported bilayers. One of the silica lenses is mounted on a sensitive leaf spring whose deflection quantifies the net force between the surfaces.

The Derjaguin Approximation relates the total integrated force between these curved surfaces (F_c) and the energy per unit area between two equivalent flat surfaces (E_f) according to $F_c = 2\pi R E_f$ (*39*, *40*). Here, *R* is the geometric average radius of the two opposed cylinders, $R = \sqrt{R_1 R_2}$, where R_1 and R_2 are the directly measured local radii of curvature of the two silica disks. As such, the measured force between the two curved disks is the sum of the interactions at all distances between curved surfaces, and this integrated force gives E_f (*23*). The radius *R* scales the magnitude of the force, but does not alter the features of the intersurface potential (*39*, *40*). This relationship holds for periodic or oscillatory forces as confirmed numerically (*23*) and experimentally (see references in refs *39* and *40*).

The SFA measurements are conducted on time scales of minutes so that we quantify adhesion under near equilibrium conditions. This differs from single molecule measurements, which are far from equilibrium (*36*). Measurements conducted at different pulling rates establish conditions where the pull-off force is independent of the loading rate. Due to lateral protein diffusion on the fluid lipid membranes, the adhesion initially changes over time. The adhesion stabilizes after ~10 min (*41*) so that our measurement time scale is >10 min. The adhesion is therefore between "equilibrated" surfaces.

When the surfaces adhere, the force to separate them, or the pull-off force, is directly related to the adhesion energy per area E_{area}. The Johnson−Kendall−Roberts theory of adhesion relates the pull-off force to the adhesion energy between deformable surfaces by $E_{area} = 2F_{po}/(3\pi R)$ (*39*, *42*). However, in the limit of very small deformations such as occurred in this study, the adhesion energy is better described by the Derjaguin−Muller−Toporov theory $E_{area} = F/(2\pi R) = 2F_{po}/(4\pi R)$ (*39*). With the surface density Γ of the cadherin molecules determined by surface plasmon resonance and radiolabeling, we estimate the energy per bond (E_b). If we assume an equilibrium distribution of bound and free ligands in the contact zone and that the adhesion energy reflects the equilibrium bond energy, then the adhesion energy is related to the individual bond energy E_b by $E_{area} = \Gamma\{E_b/[1 + \exp(-E_b/(k_B T))]\}$ where E_{area} is in units of $k_B T$/area (*43*). The bond energy can thus be estimated from the pull-off force and the protein density.

In these studies, at least two independent experiments were conducted for each cadherin interaction in Table 1. In each experiment, we conducted a minimum of three measurements (of each bond) at each of at least two regions on the sample surface. Thus, $N \geq 12$ for each of the values reported. It is important to point out that these are population average rather than single molecule measurements, so that large data sets (as in AFM measurements) are not required in order to obtain good measurement statistics.

Sample Preparation for Surface Force Measurements. The cadherins are immobilized and oriented on planar lipid bilayers supported on freshly cleaved, atomically smooth mica sheets. The mica sheets are back-coated with a ~500 Å layer of thermally evaporated silver. The mica is then glued silvered side down onto the surfaces of two opposing, hemicylindrical silica lenses. A monolayer of DPPE is deposited on the mica at 43 Å^2/lipid by Langmuir−Blodgett deposition. Onto this, we deposited a second lipid layer containing 75 mol % NTA-DLGE and 25 mol % dilauryl phosphatidyl ethanolamine (DLPE) at a surface pressure of 35 mN/m at 25 °C. This corresponds roughly to ~65 Å^2/lipid. In order to immobilize the Fc-tagged cadherins, we first formed an oriented protein A monolayer by incubating the NTA-functionalized lipid membrane with 5 μM His_6-SpA_{B2} for 1 h at room temperature (Figure 3). The His_6-SpA_{B2} chelates the Ni^{2+}-NTA headgroups via its histidine tail and forms a uniform monolayer (*44*). The unbound

Table 1: Adhesion between Canine E-Cadherin Monolayers

proteins	protein density ($\times 10^3$) cadherin/μm^2	distance, Å F/R, mN/m (energy per bond, k_BT) inner bond	 outer bond
EEC1−5Fc/EEC1−5Fc	10 ± 0.6	388 ± 5 −1.6 ± 0.3 (6.2 ± 1.0)	530 ± 5 −0.6 ± 0.1 (2.5 ± 0.4)
W2A/W2A	13 ± 1	387 ± 4 −0.67 ± 0.06 (2.2 ± 0.3)	nd[a]
D134A/D134A	13 ± 1	391 ± 5 −0.58 ± 0.11 (2.3 ± 0.4)	nd
D103A/D103A	13 ± 1	389 ± 6 −0.29 ± 0.09 (1.1 ± 0.4)	nd
D216A/D216A	13 ± 1	397 ± 4 −0.16 ± 0.08 (0.7 ± 0.3)	nd
D325A/D325A	13 ± 1	387 ± 3 −2.05 ± 0.33 (6.1 ± 1.0)	532 ± 4 −0.67 ± 0.11 (2.2 ± 0.3)
D436A/D436A	13/13	386 ± 6 −2.09 ± 0.28 (6.2 ± 1.0)	534 ± 6 −0.73 ± 10 (2.4 ± 0.4)
W2A/EEC1−5Fc	13/13	384 ± 3 −0.95 ± 0.13 (3.0 ± 0.4)	nd
D134A/EEC1−5Fc	13/13	387 ± 3 −1.05 ± 0.19 (3.2±0.7)	532 ± 3 −0.30 ± 0.05 (1.1 ± 0.2)
D103A/EEC1−5Fc	13/13	386 ± 4 −0.65 ± 0.12 (2.2 ± 0.4)†	538 ± 5 −0.33 ± 0.08 (1.3 ± 0.3)

[a] Not detected.

protein A was then washed off, and the surface was incubated with ~0.05 μM of Fc-cadherin in the same buffer for ~3 h at room temperature. The protein A fragment binds the Fc domain with nanomolar affinity (*44*). The unbound cadherin was then rinsed off, and the samples (Figure 3) were transferred underwater into the SFA chamber. Measurements were carried out with the samples bathed in buffer at a constant temperature of 25 ± 1 °C.

Quantifying Cadherin Densities by Surface Plasmon Resonance and Radiolabeling. Cadherin immobilization during the sample preparation described above was quantified by monitoring the binding in situ using a home-built surface plasmon resonance instrument (*45*). A ~38 nm gold film was deposited by thermal evaporation onto a cleaned glass slide. A self-assembled monolayer of dodecanethiol was then deposited onto this surface as described (*22*). An NTA-DLGE monolayer was deposited onto the thiol layer as described for the SFA measurements, and this assembly was mounted in the SPR fluid cell. The adsorption of the protein A and subsequent Fc-cadherin was carried out under conditions identical to those used to prepare the SFA samples. We then quantified the shifts in the resonance angle following the addition of each protein solution. The resonance curves were fit to the Fresnel reflectivity equations for a multilayer film, to yield the effective optical thickness *nd* of the protein immobilized on the surface (*46*). Here *n* and *d* are the refractive index and thickness, respectively, of the protein layer. We assumed a maximum protein thickness of 270 Å, which includes the 45 Å Fc domain and 225 Å ectodomain length. A refractive index of 1.44 was used for the protein layer to determine the surface densities. The protein densities determined from surface plasmon resonance measurements were also calibrated by quantifying the amount of ^{125}[I]-labeled cadherin bound to the monolayer (Pierce, Rockford, IL) (*46*).

RESULTS

Circular Dichrosim. The measured CD spectra of all cadherin variants investigated in this work were superimposable on the spectrum of the wild-type Fc-tagged ectodomain. The secondary structure of the proteins considered consisted of 40% beta sheet, 25% beta turn, and 35% coil. This compares with the spectral decomposition of CD data from Ig superfamily proteins, which are also beta sheet structures (*47*). By contrast, denaturation of the protein in 3 M guanidine HCl completely altered the spectra, and substantially increased the random coil content. The spectra of the denatured proteins in guanidine were the same in the presence and absence of calcium. Based on these findings, there was no obvious misfolding caused by any of the mutations investigated in this work.

Bead Aggregation Assay. Bead aggregation assays tested the adhesive activity of the different cadherin variants (*23*). Fluorescent microspheres (Bangs Laboratories) coated with wild-type ECAD formed large aggregates in a calcium-dependent fashion (Figure 4a). By contrast, control beads in the absence of calcium did not aggregate (Figure 4e). Beads coated with D436A formed large aggregates within 30 min (Figure 4b), similar to the wild-type E-cadherin coated beads. Large aggregates were also observed with D325A (Figure 4c). The W2A mutants (Figure 4d) formed smaller, but distinct aggregates. The D103A construct did not mediate any detectable aggregation above background (Figure 4f). The D134A mutant (Figure 4g) yielded a few, small aggregates, and beads coated with D216A (Figure 4h) did not show any appreciable aggregation.

Densities of Cadherin Mutants Immobilized on Protein A Functionalized Planar Bilayers. The average surface density of the proteins used in the initial surface force experiments with wt ECAD was 13 ± 1 × 10^3 cadherins/μm^2. In one set of measurements with wild-type ECAD, the use of a lower bulk protein concentration yielded a density of 10 ± 1 × 10^3 cadherins/μm^2 (Table 1). E-cadherin mutants engineered with a C-terminal human Fc domain yielded equal surface densities when immobilized under identical conditions, e.g. NTA-lipid density and bulk cadherin concentration. Since all of the mutants have the same Fc-tag, the others were assumed to yield the same surface density when immobilized under identical conditions.

Direct Force Measurements between Cadherin Monolayers. In these studies, the normalized forces were measured as a function of the membrane separation *D* during both approach and separation. In order to determine the different membrane separations at which the proteins adhere, we vary the minimum bilayer separation such that we sample all distances between ~250 Å and 600 Å. The latter is the

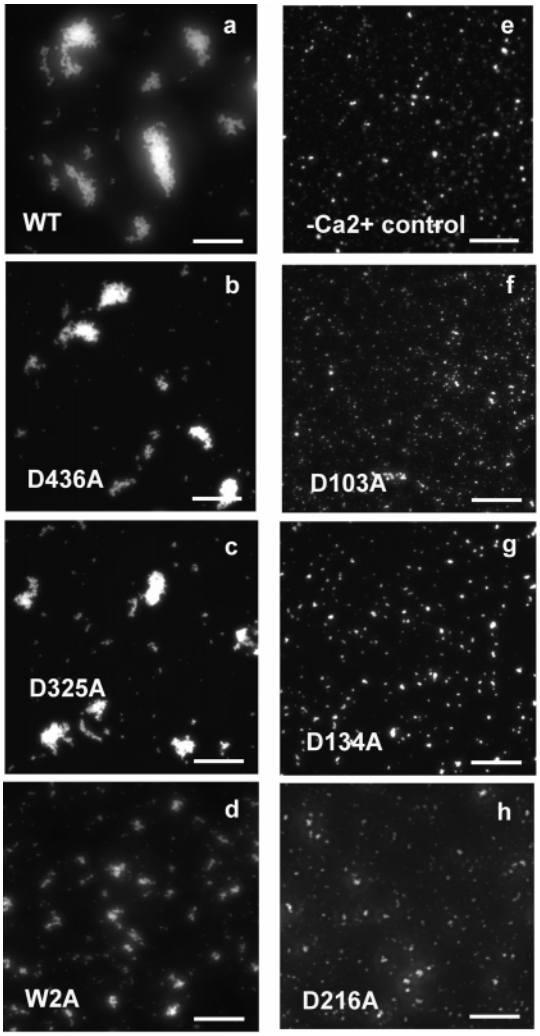

FIGURE 4: Qualitative bead aggregation assays. The protein A activated microspheres were incubated with soluble Fc-cadherin variants as described in the text, and the aggregate sizes were visualized after 30 min by bright-field microscopy. The scale bar is 50 μm. The images show the aggregate sizes measured with (a) wild-type cadherin ectodomains, (b) D436A, (c) D325A, (d) W2A, (e) $-Ca^{2+}$ control, (f) D103A, (g) D134A mutants, and (h) D216A.

smallest separation achieved before the surfaces are pulled apart. During separation, the surfaces move smoothly out of contact unless the proteins adhere. If they adhere, then the receding force curve drops to negative values. At the minimum force or maximum attraction, the bonds yield and the surfaces pull out of contact. In these measurements, after the final pull-off and jump out of contact, the final resting position is at $D > 600$ Å. With the wild-type ectodomain, the adhesive minima were at either of two unique distances. The spring deflection at the point of adhesive failure gives the pull-off force.

Opposing wild-type E-cadherin ectodomains formed two homophilic bonds at membrane separations of 388 ± 5 Å and 530 ± 13 Å (Figure 5). During approach, the cadherin layers contact via their outer tips was at $D < 570$ Å. This agrees with the combined measured 15 Å thickness of the protein A layer, the 45 Å thickness of the Fc fragment, and the 225 Å cadherin ectodomain length ($570 = 2(15 + 45 + 225)$) (cf. Figure 3). From these distances and prior domain deletion studies (*24*), we inferred the relative protein alignments at 388 Å and at 530 Å. The adhesion at 388 Å

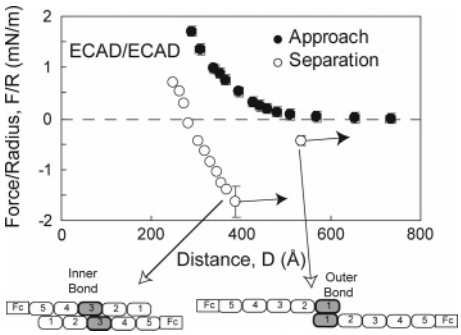

FIGURE 5: Normalized force−distance profiles between identical, wild-type E-cadherin ectodomain monolayers. The filled circles indicate the normalized force vs the distance D between cadherin monolayers during approach (decreasing D). Open circles show the force curves measured during separation and the positions and magnitudes of the adhesive minima ($F/R < 0$). The out arrows indicate the starting positions at which the protein−protein bonds yield and the surfaces jump out of contact. The spring constant was 217 N/m.

corresponds to EC3/EC3 overlap, and the bond at 530 Å corresponds to adhesive contact between EC1 domains. In these studies and in previous measurements with C-CAD, no additional adhesive interactions occur when the minimum approach distance is <360 Å. The magnitude of the compressive force ($F > 0$) does not affect the findings, unless it is high enough to crush the protein.

At 388 Å the adhesive force was -1.6 ± 0.3 mN/m, and at 530 Å the adhesion was -0.6 ± 0.1 mN/m. The average energy per bond, E_b, was then estimated as described above. Here Γ is the measured surface density of $10 \pm 1 \times 10^3/\mu m^2$ of the Fc-cadherin used in the experiment, and F_{po} is the pull-off force. The thus estimated energies per bond were $6.2 \pm 1\ k_BT$ and $2.5 \pm 0.4\ k_BT$, respectively, where k_B is the Boltzmann constant and T is the absolute temperature. These results are summarized in Table 1.

Figure 6a shows the normalized force versus distance profile between the W2A mutants at $13 \pm 1 \times 10^3/\mu m^2$. The surfaces were first brought to $D < 370$ Å such that the cadherin ectodomains fully overlapped. When separated from that position, the proteins adhered at $D = 387 \pm 4$ Å. The magnitude of the pull-off force was $F_{po}/R = -0.67 \pm 0.06$ mN/m, and E_b was $2.2 \pm 0.2\ k_BT$. When the W2A monolayers were brought to distances $D > 400$ Å where EC3/EC3 contacts cannot occur, there was no detectable hysteresis in the receding curve and there was no measured adhesion. Binding between the outer EC1 domains, as observed with the wild-type E-cadherin, was completely absent.

In addition to the weak adhesion at 387 Å, in some cases, the W2A monolayers spontaneously jumped into contact at ~350 Å from all distances between $390 < D < 540$ Å. This depended on the spring stiffness since the jump-in occurs when the gradient of the intersurface potential exceeds the spring constant (*48*). Between W2A mutants, with a spring constant of 217 N/m, the broken inward line indicates the jump to contact at ~350 Å (Figure 6a). With a stiffer spring ($k_s = 489$ N/m), the jump-in did not occur, indicating that the potential gradient is <489 N/m. Under conditions where these jumps occur, it is not possible to detect intermediate bonds. However, even with the stiffer spring where there was no jump to contact, there was no additional binding.

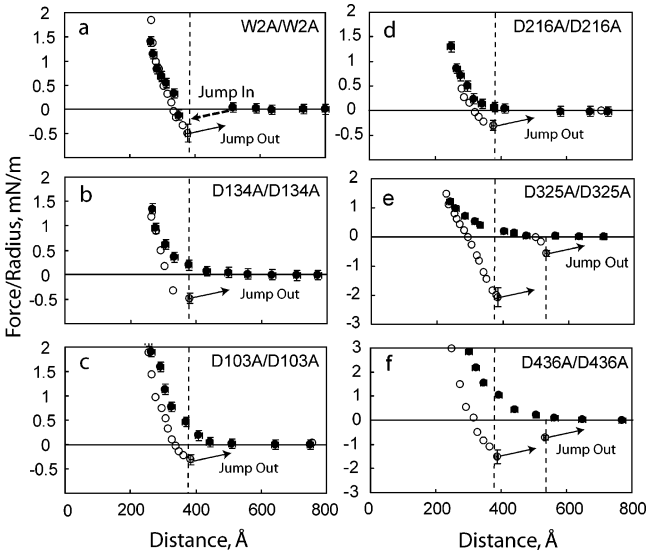

FIGURE 6: Normalized force−distance profiles between identical E-cadherin monolayers. Data are shown for (a) W2A (b) D134A, (c) D103A, (d) D216A, (e) D325A, and (f) D436A mutants. The filled circles indicate the normalized force vs the distance D between cadherin monolayers during approach (decreasing D). Open circles show the forces measured during separation and the positions and magnitudes of the adhesive minima ($F/R < 0$). The vertical dashed lines mark the average position from which the proteins pulled out of adhesive contact. The out arrows show the positions at which the protein−protein bonds yield and the surfaces jump out of contact. The spring constant was 217 N/m in all measurements (a−f).

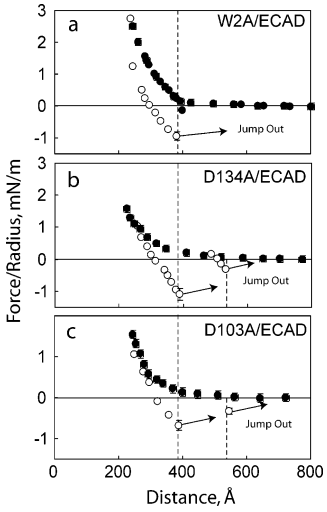

FIGURE 7: Normalized force−distance profiles between wild-type E-cadherin and E-cadherin mutants. Data show the heterophilic force−distance profile between ECAD and (a) W2A, (b) D134A, and (c) D103A. The filled circles indicate the normalized force vs the distance profiles measured during approach (decreasing D). Open circles show forces during separation and the positions and magnitudes of the adhesive minima ($F/R < 0$). The vertical dashed lines mark the average position from which the proteins pulled out of adhesive contact. The out arrows show the positions where the surfaces jump out of contact. The spring constant was 217 N/m in all measurements (a−c).

Figure 6b shows the normalized force−distance profile between opposed monolayers of the D134A mutant. Similar to the W2A mutant, the proteins adhered weakly at 391 ± 5 Å with a pull-off force of $F_{po}/R = -0.58 \pm 0.11$ mN/m (Table 1). This gives an estimated energy per bond of 2.0 ± 0.3 k_BT. The position of the maximum adhesive force also coincides with aligned, antiparallel EC3 domains, but this adhesion is much weaker than that of EEC1−5Fc at the same distance (Table 1). There was no detectable adhesion or hysteresis at any other membrane distance. Thus, the inner, putative EC3/EC3 bond survives in this mutant, but it is significantly attenuated. At the same time, the outer EC1/EC1 bond is absent. In contrast with the W2A mutant, there was no detectable spontaneous jump-in observed with the D134A mutant.

The mutant D103A also adhered at 389 ± 6 Å, with even weaker adhesion of −0.29 ± 0.09 mN/m (Figure 6c, Table 1). This corresponds to an average energy per bond of 1.1 ± 0.4 k_BT. This is statistically lower than that of the wild-type protein and of D134A ($p < 0.001$). The outer putative EC1/EC1 bond was also absent in this case. Similarly, the D216A mutation completely abolished the outer bond at 530 Å, and substantially attenuated the adhesion at 388 ± 7 Å (Figure 6d) (Table 1). The pull-off force at 388 Å was −0.16 ± 0.08 mN/m, which corresponds to the average bond energy of 0.7 ± 0.3 k_BT. This is lower than the inner bond of both the wild-type protein and the D103A mutant ($p = 0.002$). There was no additional binding detected at any other distance.

Both D325A and D436A with DXXA mutations at the EC34 and EC45 junctions, respectively, bound at two distances. The D325A variant adhered at 387 ± 3 Å and 532 ± 4 Å with adhesive forces of −2.05 ± 0.33 mN/m and −0.67 ± 0.11 mN/m, respectively (Figure 6e). These values correspond to bond energies of 6.1 ± 1 k_BT and 2.2 ± 0.3 k_BT for the respective inner and outer bonds. These values are not statistically different from that of the wild-type protein with $p = 0.90$ and $p = 0.28$ for the inner and outer bonds, respectively. Likewise, the D436A mutant bound at 386 ± 6 Å and 534 ± 6 Å with corresponding pull-off forces of −2.09 ± 0.28 and −0.73 ± 0.10 mN/m (Figure 6f, Table 1). Again, the average bond energies were statistically the same as for the wild-type protein with $p = 0.70$ and $p = 0.71$ for the inner and outer bonds, respectively.

We tested the ability of the canine EEC1−5Fc mutants to bind to wild-type EEC1−5Fc, in order to determine whether the unmodified protein rescued some of the binding capacity in reciprocal cadherin interactions. Figure 7a−c shows the force−distance profiles measured between wild-type ECAD ectodomains and the W2A, D134A, and D103A mutants. When the W2A monolayer was brought close to EEC1−5Fc, the two surfaces spontaneously jumped into contact at 350 ± 20 Å (Figure 7a). Upon separation, the maximum attractive force and pull-off were at 384 ± 3 Å. The measured adhesion was −0.95 ± 0.13 mN/m, which corresponds to 3.0 ± 0.4 k_BT per bond (Table 1). This average bond energy exceeds that between W2A mutants ($p = 0.002$).

In contrast, the D134A and D103A variants bound wild-type EEC1−5Fc at two membrane distances. Figure 7b shows the force profile between immobilized D134A and wild-type EEC1−5Fc. The proteins adhered at 387 ± 3 Å with a normalized force of −1.05 ± 0.19 mN/m, and at 532 ± 3 Å with an adhesive force of −0.30 ± 0.05 mN/m. The average bond energies are 3.2 ± 0.7 k_BT and 1.1 ± 0.2 k_BT, respectively (Table 1). The values were statistically higher than the adhesion between D134A mutants with $p < 0.001$ in both cases, but weaker than the adhesion between wild-type ectodomains. Similarly, D103A bound wild-type

EEC1−5Fc at 386 ± 4 Å and 538 ± 5 Å with the respective adhesions of −0.65 ± 0.12 mN/m and −0.33 ± 0.08 mN/m (Figure 7c). The latter correspond to bond energies of 2.2 ± 0.4 k_BT and 1.3 ± 0.3 k_BT (Table 1). Again, these values were lower than adhesion between wild-type ectodomains ($p < 0.001$) but higher than between identical mutants ($p < 0.001$).

DISCUSSION

The new finding in this study is the evidence for structural cooperativity and allostery in the full cadherin ectodomain. The impact of the W2A mutation on EC3-mediated adhesion suggests that W2 acts as an allosteric regulator of cadherin function. In the context of ligand binding, allostery refers to the ability of ligand binding to affect distal sites in the protein that are separated from the ligand binding site by several amino acids (*49*). In the undocked state, W2 is free on the N-terminus of the unstructured A strand of a beta sheet (*11*, *15*), and is highly unlikely to have any allosteric effects. However, docking in the hydrophobic pocket induces structural changes in the EC1 domain(*12*). Here we show that W2A both abrogates the outer adhesive bond and reduces the strength of the bond at 387 ± 4 Å 3-fold. The latter might seem a modest effect, except that a 3-fold change in bond energy gives a $\sim e^3 = 20$ change in affinity. This cannot be explained by folding since the W2A mutation does not destabilize the protein structure. The CD spectra are the same as for the wild-type ectodomain. The reduced EC3-mediated adhesion following the loss of tight W2 docking is evidence for the allosteric influence of W2 binding.

The Trp2 can dock to the hydrophobic pocket of the same molecule, an adjacent protein (cis), or an opposed protein (trans) (*10*, *14*−*16*, *50*, *51*). Currently there are no results that show how W2A affects beta strand exchange at the atomic scale. However, preventing hydrogen bonding between W2ϵ and D90O increases the W2 exchange rate (*51*). Furthermore, in steered molecular dynamics simulations, the alanine of W2A easily pulls out of the hydrophobic pocket (*52*). That W2A disrupts docking argues that the destabilization of ligand (typtophan) binding prevents the allosteric activation of the second EC3-mediated adhesive bond.

Allostery in cadherin domains is not unprecedented. A previous report demonstrated structural coupling between the W2 binding pocket and the calcium site at D134 in the EC1 domain of N-cadherin (*12*). W2 docking induced conformational changes near the calcium binding sites. Conversely, both the D134A mutation and low calcium affect W2 docking. Allatia reported calcium binding cooperativity within a single EC1/EC2 junction (*31*). These force data provide evidence for much longer range allostery in the full ectodomain.

These results may resolve, in part, controversy concerning the identities of the functional adhesive domains of classical cadherins. One of the puzzles regarding the multidomain binding mechanism has been the inability to identify, by more conventional methods, additional bound states involving domains other than EC1. Notably, the W2A mutant eliminates the aggregation of cells in stirred suspensions. Our findings show that altering EC1 impairs both the N-terminal EC1 and EC3 domain functions. Thus, attempts to expose additional functional sites by removing or mutating EC1 may inadvertently compromise the function of other regions on the protein.

The nonlocal effects of the calcium site mutations are also evidence for structural cooperativity. That is, mutations intended to affect the local protein structure in fact impact distant sites on the molecule (*49*). A recent study of polyproteins showed that interactions between adjacent domains affect their folding kinetics and stability (*53*). Because the stiff calcium linkers couple adjacent beta structures, it is not entirely surprising that the calcium mutation at the EC1/EC2 junction, for example, affects EC1 function. However, it is not obvious that it would also alter the function of EC3, which is separated by a full domain and an additional calcium bridge. Similarly, although the effect of the D216A mutation on EC3 might be anticipated, the impact on EC1 binding is more surprising. The impact of the calcium site mutations is also context dependent. Although D325A affects the EC3/EC4 junction, it has no statistically significant effect on either of the two adhesive bonds. Likewise, D436A, which is as close to EC3 as the D216A mutation is to EC1, does not affect either bond.

Previous findings also suggest structural coupling between the domains. Removing EC4 and EC5 affects the population average outer, i.e. EC1−EC1 bond strength of C-cadherin (*24*). The increase in EC12 mediated cell adhesion relative to EC1 may be due to similar effects (*54*). Interdomain cooperativity is well-known in integrins and Ig superfamily proteins (*55*).

The four mutants W2A, D103A, D134A, and D216A abolished the outer EC1/EC1 bond. However, both W2A and D134A still exhibit appreciable adhesion at 382 ± 4 Å with bond energies 2.2k_BT and 2.3k_BT, respectively. Based on the binding distance and prior work (*24*), this residual adhesion is attributed to EC3. Binding was unexpected since both mutants were apparently nonfunctional in cell aggregation assays (*32*). Our bead aggregation results, however, confirm that both proteins aggregate Brownian particles (microspheres). The low bond energies must therefore exceed the thermal energy k_BT, in agreement with these force measurements (Table 1).

Differences in the assay methods used can account for this apparent discrepancy. In the cell aggregation assays, cells are kept suspended by agitating the solutions at mixing speeds of >70 rpm for 30−45 min (*16*, *21*, *32*, *56*, *57*). These suspended cells are constantly subject to shear forces, which can disrupt interparticle bonds. As a result, cell aggregation patterns depend on the mixing rates such that aggregates formed at mixing speeds of 10 rpm differed from those formed at mixing rates of 70−100 rpm (*56*, *58*). This dependence is expected since the shear, which increases with the mixing speed, alters the particle aggregation behavior (*59*, *60*). Thus, the mixing rate sets the (undefined) threshold for cadherin bond strengths needed to aggregate cells under the assay conditions. By contrast, in bead aggregation assays, Brownian forces keep the beads suspended, and bonds exceeding the thermal energy k_BT cause aggregation (*40*). The SFA can quantify bonds with energies less than k_BT, even though the latter might be insufficient to aggregate beads, e.g. $<k_BT$ (*36*, *61*). We therefore attribute the apparently different findings to the threshold detection limits of the different approaches. With the SFA, bead aggregation, and cell aggregation measurements, the thresholds are

roughly $0.5k_BT$, $>1k_BT$, and the (unknown) shear force, which can rupture bonds $\gg k_BT$.

Although they are widely used, neither cell aggregation nor bead aggregation assays actually quantify adhesion. Bond association and dissociation kinetics control aggregation (*40*). Shear forces in stirred suspensions also affect the bond kinetics, and hence the aggregation behavior (*59*, *60*). If the association rates are similar, aggregate sizes qualitatively indicate the relative bond strengths of protein bonds subject to Brownian forces or shear. Thus aggregate sizes should only be used as a qualitative indicator of the relative ability of proteins to aggregate particles (or cells). The bead assay results described here qualitatively support the conclusions of the quantitative force data.

Previous reports of both cell aggregation (100 rpm) and wound-healing assays documented the impact of cadherin point mutations at the DXXD motifs at each EC domain junction (D103A, D216A, D325A, and D436A) (*32*). The D103A and the D216A mutants significantly reduced cell aggregation relative to the wild-type protein. D325A showed only a slight reduction, and the D436A mutant did not differ detectably from the wild-type human E-cadherin.

In the wound-healing assay, a monolayer of cadherin expressing cells is disrupted in one area and surrounding cells migrate into that region. Because only D216A increased cell migration rates in those motility assays, it was deemed to be the most critical of the DXXD mutations (*32*). Our finding is consistent with their conclusion. The mechanism by which the loss of E-cadherin adhesion increases motility is not known, but these findings reveal the molecular level consequences of this critical mutation.

In cell studies, the D103A and D216A mutants primarily exhibited perinuclear localization while D325A, D436A, and wild-type ECAD localize at cell−cell junctions (*32*). These force data map the differences in localization to quantitative differences in protein adhesion. They suggest that abnormal cadherin localization is a *consequence* rather than the *cause* of impaired binding, and that outside-in signaling related to the bond strength may direct localization.

The reciprocal binding between the wild-type protein and three mutants (W2A, D103A, and D134A) shows that proteins with Trp2, which could hydrogen bond to Glu90 in a functional EC1 pocket, do form trans EC1 bonds (*10*, *52*). In principle, this should occur, because, in the asymmetric case, there is an intact Trp2 opposite a functional hydrophobic pocket. Since the W2 side chain is intact, we correctly predicted that the mutant would bind a wild-type ectodomain. We could not, however, establish whether the mutations alter the intrinsic bond strength or the equilibrium distribution of bound and free states, since the SFA measures the population average properties. Single bond rupture measurements could resolve the latter issue, since they probe intrinsic (single) bond strengths (*25*, *26*).

The EC1 of W2A failed to bind the wild-type ectodomain. Nevertheless, we might expect half of the strand dimer to form. Steered molecular dynamics simulations showed that the forced dissociation of the Ala2 side chain of the W2A mutant from the hydrophobic pocket is very facile (*52*). Thus, the bond may be too unstable to generate detectable adhesion.

In conclusion, these findings make three central points. First, mutations at calcium binding sites in the outer three EC domains affect both of the two bound states measured between canine E-cadherin ectodomains. This reveals structural coupling between cadherin domains. Second, the effect of the W2A mutant suggests that Trp2 may function as an allosteric regulator of cadherin adhesion. This may in turn explain apparent discrepancies between force measurements and prior mutagenesis studies. Third, the force measurements reveal the molecular changes due to calcium binding sites mutations that underlie associated changes in cell aggregation and cell motility in gastric cancers.

ACKNOWLEDGMENT

We thank Saiko Rosenberger for her excellent technical assistance.

REFERENCES

1. Gumbiner, B. M. (2005) Regulation of Cadherin-mediated Adhesion in Morphogenesis, *Nat. Rev.: Mol. Cell Biol. 6*, 622−634.
2. Gumbiner, B. M. (1996) Cell Adhesion: The Molecular Basis of Tissue Architecture and Morphogenesis, *Cell 84*, 345−357.
3. Takeichi, M. (1995) Morphogenetic roles of classic cadherins, *Curr. Opin. Cell Biol. 7*, 619−627.
4. Takeichi, M. (1993) Cadherins in cancer: implications for invasion and metastasis, *Curr. Opin. Cell Biol. 5*, 806−811.
5. Handschuh, G., Candidusand, S., Luber, B., Reich, U, Schott, C., and Oswald, S. (1999) Tumor associated E-cadherin mutations alter cellular morphology, decrease cellular adhesion, and increase cellular motility, *Oncogene 18*, 4301−4312.
6. Becker, K. F., Atkinson, M. J., Reich, U., Becker, I., Nekarda, H., Siewert, J. R., and Hofler, H. (1994) E-cadherin gene mutations provide clues to diffuse type gastric carcinomas, *Cancer Res. 54*, 3845−3852.
7. Yap, A. S., Brieher, W. M., and Gumbiner, B. M. (1997) Molecular and Functional Analysis of Cadherin-Based Adherens Junctions, *Annu. Rev. Cell. Dev. Biol. 13*, 119−146.
8. Nagar, B., Overduin, M., Ikura, M., and Rini, J. M. (1995) Structural basis of calcium-induced E-cadherin rigidification and dimerization, *Nature 380*, 360−364.
9. Pokutta, S., Herrenknecht, K., Kemler, R., and Engel, J. (1994) Conformational changes of the recombinent extracellular domain of E-cadherin upon calcium binding, *Eur. J. Biochem. 223*, 1019−1026.
10. Boggon, T., Murray, J., Chappuis-Flament, S., Wong, E., Gumbiner, B. M., and Shapiro, L. (2002) C-cadherin ectodomain structure and implications for cell adhesion mechanisms, *Science 296*, 1308−1313.
11. Haussinger, D., Ahrens, T., Sass, H.-J., Pertz, O., Engel, J., and Grzesiek, S. (2002) Calcium-dependent Homoassociation of E-cadherin by NMR Spectroscopy: Changes in Mobility, Conformation, and Mapping of Contact Regions, *J. Mol. Biol. 324*, 823−839.
12. Harrison, O. J., Corps, E. M., Berge, T., and Kilshaw, P. J. (2004) The mechanism of cell adhesion by classical cadherins: the role of domain 1, *J. Cell Sci. 118*, 718−721.
13. Shapiro, L., Fannon, A. M., Kwong, P. D., Thompson, A., Lehmann, M. G., Grübel, G., Legrand, J.-F., Als-Nielsen, J., Colman, D. R., and Hendrickson, W. A. (1995) Structural basis of cell−cell adhesion of cadherins, *Nature 374*, 327−337.
14. Troyanovsky, R. B., Sokolov, E., and Troyanovsky, S. M. (2003) Adhesive and Lateral E-Cadherin Dimers are Mediated by the Same Interface, *Mol. Cell. Biol. 23*, 7965−7972.
15. Pertz, O., Bozic, A., Koch, W., Fauser, C., Brancaccio, A., and Engel, J. (1999) A new crystal structure, Ca^{2+} dependence and mutational analysis reveal molecular details of E-cadherin homoassociation, *EMBO J. 18*, 1738−1747.
16. Tamura, K., Shan, W.-S., Hendrickson, W. A., Colman, D. R., and Shapiro, L. (1998) Structure-Function Analysis of Cell Adhesion by Neural (N-) Cadherin, *Neuron 20*, 1153−1163.
17. Ozawa, M. (2002) Lateral Dimerization of the E-cadherin Extracellular Domain is Necessary but Not Sufficient for Adhesive Activity, *J. Biol. Chem. 22*, 19600−19608.
18. Klingelhofer, J., Laur, O. Y., Troyanovsky, R. B., and Troyanovsky, S. M. (2002) Dynamic interplay between adhesive and lateral E-cadherin dimers, *Mol. Cell. Biol. 22*, 7449−7458.

19. Perret, E., Benoliel, A. M., Nassoy, P., Pierres, A., Delmas, V., Thiery, J.-P., Bongrand, P., and Feracci, H. (2002) Fast dissociation kinetics revealed by flow chamber analysis, *EMBO J. 21*, 2537−2546.
20. Nose, A., Tsuji, K., and Takeichi, M. (1990) Localization of specificity determining sites in cadherin cell adhesion molecules, *Cell 61*, 147−155.
21. Shan, W. S., Tanaka, H., Phillips, G. R., Arndt, K., Yoshida, M., and Colman, D. R. (2000) Functional cis-heterodimers of N- and R-cadherins, *J. Cell Biol. 148*, 579−590.
22. Sivasankar, S., Brieher, W., Lavrik, N., Gumbiner, B., and Leckband, D. (1999) Direct Molecular Force Measurements of Multiple Adhesive Interactions Between Cadherin Ectodomains, *Proc. Natl. Acad. Sci. U.S.A. 96*, 11820−11824.
23. Sivasankar, S., Gumbiner, B., and Leckband, D. (2001) Direct Measurements of Multiple Adhesive Alignments and Unbinding Trajectories between Cadherin Extracellular Domains, *Biophys. J. 80*, 1758−1768.
24. Zhu, B., Chappuis-Flament, S., Wong, E., Jensen, I., Gumbiner, B. M., and Leckband, D. E. (2003) Functional Analysis of the Structural Basis of Homophilic Cadherin Adhesion, *Biophys. J. 41*, 12163−12170.
25. Bayas, M., Leung, A., Evans, E., and Leckband, D. (2006) Lifetime Measurements Reveal Kinetic Differences between Homophilic Cadherin Bonds, *Biophys. J. 90*, 1385−1395.
26. Perret, E., Leung, A., Feracci, H., and Evans, E. (2005) Homophilic Cadherin Interactions Show a Surprising Hierarchy of Mechanical Strengths, *Proc. Natl. Acad. Sci. U.S.A. 101*, 16472−16477.
27. Chappuis-Flament, S., Wong, E., Hicks, L. D., Kay, C. M., and Gumbiner, B. M. (2001) Multiple cadherin extracellular repeats mediate homophilic binding and adhesion, *J. Cell Biol. 154*, 231−243.
28. Renaud-Young, M., and Gallin, W. J. (2002) In the First Extracellular Domain of E-cadherin, Heterophilic Interactions, but Not the Conserved His-Ala-Val Motif, Are Required for Adhesion, *J. Biol. Chem. 277*, 39609−39616.
29. Guilford, P., Hopkins, J., Harraway, J., McLeod, M., Harawira, P., Taite, H., Scoular, R. Miller, A., and Reeve, A. E. (1998) E-cadherin germline mutations in familial gastric cancer, *Nature 392*, 402−405.
30. Koch, A. W., Pokutta, S., Lustig, A., and Engel, J. (1997) Calcium binding and homoassociation of E-cadherin domains, *Biochemistry 36*, 7697−7705.
31. Alattia, J.-R., Ames, J. B., Porumb, T., Tong, K. I., Heng, Y. M., Ottensmeyer, P., Kay, C. M., and Ikura, M. (1997) Lateral self-assembly of E-cadherin directed by cooperative calcium binding, *FEBS Lett. 417*, 405−408.
32. Handschuh, G., Luber, B., Hutzler, P., Hofler, H., and Becker, K. F. (2001) Single amino acid substitutions in conserved extracellular domains of E-cadherin differ in their functional consequences, *J. Mol. Biol. 314*, 445−454.
33. Chen, Y. T., and Nelson, W. J. (1996) Continuous Production of Soluble Extracellular Domain of a Type-I Transmembrane Protein in Mammalian Cells Using an Epstein−Barr Virus Ori-P−Based Expression Vector, *Anal. Biochem. 242*, 276−278.
34. Woody, R. W. (1995) *Circular Dichroism*, Academic Press, New York.
35. Sreerama, N., and Woody, R. W. (2000) Estimation of Protein Secondary Structure from Circular Dichroism Spectra: Comparison of CONTIN, SELCON, and CDSSTR Methods with an Expanded Reference Set, *Anal. Biochem. 287*, 252−260.
36. Leckband, D., and Israelachvili, J. N. (2001) Intermolecular Forces in Biology, *Q. Rev. Biophys. 34*, 105−267.
37. Israelachvili, J. (1973) Thin Film Studies Using Multiple-Beam Interferometry, *J. Colloid Interface Sci. 44*, 259−272.
38. Martel, L., Johnson, C., Boutet, S., Al-Kurdi, R., Konovalov, O., Robinson, I., Leckband, D., and Legrand, J.-F. (2002) X-Ray reflectivity investigations of two-dimensional assemblies of C-cadherin: First steps in structural and functional studies, *J. Phys. IV 12*, 365−377.
39. Israelachvili, J. (1992) *Intermolecular and Surface Forces*, 2nd ed., Academic Press, New York.
40. Hunter, R. (1989) *Foundations of Colloid Science*, Vol. 1, Oxford University Press, Oxford.
41. Leckband, D., Schmitt, F.-J., Israelachvili, J., and Knoll, W. (1994) Direct force measurements of specific and nonspecific protein interactions, *Biochemistry 33*, 4611−4624.
42. Johnson, K. L., Kendall, K., and Roberts, A. D. (1971) Surface energy and the contact of elastic solids, *Proc. R. Soc. London A 324*, 301−313.
43. Tereste, D., Pincet, F., Brellier, M., Mioskowski, C., and Perez, E. (2005) The Binding Energy of Two Nitrilotriacetate Groups Sharing a Nickel Ion, *J. Am. Chem. Soc. 127*, 3879−3884.
44. Johnson, C., Prakasam, A., Jensen, I., Vijayendran, R., and Leckband, D. (2002) Engineered protein A for the orientational control of immobilized proteins, *Bioconjugate Chem. 14*, 974−978.
45. Lavrik, N., and Leckband, D. (2000) Optical and direct force measurements of the interaction between monolayers of aromatic macrocycles on surfactant monolayers, *Langmuir 16*, 1842−1851.
46. Yeung, C., Purves, T., Kloss, A. A., Kuhl, T. L., Sligar, S., and Leckband, D. (1999) Cytochrome *c* Recognition of Immobilized, Orientational Variants of Cytochrome b5: Direct Force and Equilibrium Binding Measurements, *Langmuir 15*, 6829−6836.
47. Tetin, S. Y., Prendergast, F. G., and Venyaminov, S. Y. (2003) Accuracy of protein secondary structure determination from circular dichroism spectra based on immunoglobulin examples, *Anal. Biochem. 321*, 183−187.
48. Marra, J., and Israelachvili, J. (1985) Direct Measurements of Forces between Phosphatidylcholine and Phosphatidylethanolamine bilayers in Aqueous Electrolyte Solutions, *Biochemistry 24*, 4608−4618.
49. Creighton, T. E. (1993) *Proteins: Structures and Molecular Properties*, 2nd ed., WH Freeman and Company, New York.
50. Koch, A. W., Faroc, A., Shan, W., Zeng, L., Colman, D. R., and Zhou, M.-M. (2004) Structure of the Neural (N-) Cadherin Prodomain Reveals a Cadherin Extracellular Domain-like Fold without Adhesive Characteristics, *Structure 12*, 793−805.
51. Haussinger, D., Ahrens, T., Engel, J., Stetefeld, J., and Grzesiek, S. (2004) Proteolytic E-Cadherin activation followed by solution NMR and X-ray crystallography, *EMBO J. 23*, 1699−1708.
52. Bayas, M., Schulten, K., and Leckband, D. (2004) Forced Rupture of the Strand-dimer Interface between C-cadherin Ectodomains, *Mech. Chem. Biosyst. 1*, 101−111.
53. Rounsevell, W. S. R., Steward, A., and Clarke, J. (2005) Biophysical Investigations of Engineered Polyproteins: Implications for Force Data, *Biophys. J. 88*, 2022−2029.
54. Shan, W., Yagita, Y., Wang, Z., Koch, A., Svenningsen, A. F., Gruzglin, E., Pedraza, L., and Colman, D. R. (2004) The Minimal Essential Unit for Cadherin-mediated Intercellular Adhesion Comprises Extracellular Domains 1 and 2, *J. Biol. Chem. 279*, 55914−55923.
55. Hynes, R. O. (2002) Integrins: bidirectional, allosteric signaling machines, *Cell 110*, 673−687.
56. Duguay, D., Foty, R. A., and Steinberg, M. S. (2003) Cadherin-mediated cell adhesion and tissue segregation: qualitative and quantitative determinants, *Dev. Biol. 253*, 309−323.
57. Nose, A., Nagafuchi, A., and Takeichi, M. (1988) Expressed recombinant cadherins mediate cell sorting in model systems, *Cell 54*, 147−155.
58. Foty, R. A., and Steinberg, M. S. (2004) The differential adhesion hypothesis: a direct evaluation, *Dev. Biol. 278*, 255−263.
59. Laurenzi, I. J., and Diamond, S. L. (1999) Monte Carlo Simulation of the Heterotypic Aggregation Kinetics of Platelets and Neutrophils, *Biophys. J. 77*, 1733−1746.
60. Goldsmith, H. L., Quin, A. T., Drury, G., Spanos, C., McIntosh, F. A., and Simon, S. I. (2001) Dynamics of Neutrophil Aggregation in Couette Flow Revealed by Videomicroscopy: Effect of Shear Rate on Two-Body Collision Efficiency and Doublet Lifetime, *Biophys. J. 81*, 2020−2034.
61. Israelachvili, J., and McGuiggan, P. (1990) Adhesion and short-range forces between surfaces: New apparatus for surface force measurements, *J. Mater. Res. 5*, 2223−2231.

BI060213M